2020 American Control Conference
Denver, CO, USA, July 1-3, 2020

Battery Internal Short Detection Methodology Using Cell Swelling Measurements

Ting Cai, Sravan Pannala, Anna G. Stefanopoulou and Jason B. Siegel

***Abstract*—Li-ion battery internal short circuits are a major safety issue for electric vehicles, and can lead to serious consequences such as battery thermal runaway. An internal short can be caused by mechanical abuse, high temperature, overcharging, and lithium plating. The low impedance or hard internal short circuit is the most dangerous kind. The high internal current flow can lead to battery temperature increase, thermal runaway, and even explosion in a few seconds. Algorithms that can quickly detect such serious events with a high confidence level and which are robust to sensor noise are needed to ensure passenger safety. False positives are also undesirable as many thermal runaway mitigation techniques, such as activating pyrotechnic safety switches, would disable the vehicle. Conventional methods of battery internal short detection, including voltage and surface temperature based algorithms, work well for a single cell. However, these methods are difficult to apply in large scale battery packs with many parallel cells. In this study, we propose a new internal short detection method by using cell swelling information during the early stages of a battery heating caused by an internal short circuit. By measuring cell expansion force, higher confidence level detection can be achieved for an internal short circuit in an electric vehicle scale battery pack.**

I. Introduction

LITHIUM ion batteries are widely used in energy storage and electric vehicles. However, the growth in battery energy density increases the risk and severity of battery failures. Many of the battery accidents start with an overcharge, overheat, mechanical abuse [1] or lithium plating that lead to battery internal short circuit (ISC). Joule heating, caused by an ISC event, can elevate the battery temperature to thermal runaway critical temperature [2]. At this temperature, battery side reactions will be active, and will quickly produce additional heat and can lead to battery thermal runaway. Common hazards of battery thermal runaway include toxic off-gassing, smoke, fire, and even an explosion [3]. Detection of an ISC event should be made early to avoid further damages.

Previous methods of detecting ISC are usually based on voltage or current measurement. Voltage based methods work well with a single cell, and most battery abuse testing shows significant battery voltage drop [4], [5]. Xia [6] proposed a fault-tolerant method that can distinguish between cell failure and voltage sensor failure. The fault detection can be model free with correlation coefficient calculated for neighboring cells in series [7]. The model also features fast detection speed, as the voltage drop is almost instantaneous after an ISC [8]. In electric vehicle battery packs, the batteries are connected in parallel. For example, the Tesla Model 3 battery packs come with 46 cells in parallel, and the Tesla Roadster has 69 cells in parallel. The large number of parallel connected batteries will suppress the battery fault voltage signal. As the other healthy cells in parallel will continually supply nominal voltage, the pack voltage with a single cell at fault will be very similar to healthy battery packs voltage, making the fault detection using voltage alone more challenging.

Zhang [9] proposed an ISC detection method based on symmetrical loop circuit topology. The method is effective for large scale battery packs, and fast in detection time. However, the method requires additional current sensors to monitor the current of individual cells which is cost prohibitive. Other methods of ISC detection using voltage, current and surface temperature measurements can be found in [10], [11], [12]. These fault detection methods work well with soft ISC, where the temperature gradient inside the cell is not huge.

For hard ISC, the battery internal temperature can be elevated in a few seconds, causing huge temperature gradient inside the cell. Prior works divided the battery into three temperature sections [13], [14], and showing that at early stage of ISC, the battery ISC region has a higher temperature. Surface temperature rise for such event is slower than voltage drop and expansion force rise.

Other detection methods, such as gas detection, aim at the vented gas during the thermal runaway process [15]. Previous studies from Lammer [16] showed a large amount of CO_2 is released with the first venting during a thermal runaway event. The gas detection method can also be effective when the BMS is not active or connected to the cells. In a prior work, for a battery storage drum, gas detection method targeted at CO_2 concentrations shows much faster detection speed than temperature monitoring at drum surface [17].

This study proposes an ISC detection method based on expansion force measurement. In a hard internal short event, high temperature and battery side reactions in the ISC region will produce a large amount of gas. This leads to a quick cell swelling and a sudden increase of expansion force [14]. In a battery pack, with many cells stacked together, the force fault signal due to swelling in a singe cell can be easily detected. In the proposed algorithm, we build an observer for the cell expansion force in normal operating conditions. The observer value is compared with online force measurement. An alarm will be triggered when the deviation of the observer value and the measurement exceeds a threshold. The simulation results

Ting Cai, Sravan Pannala, Anna G. Stefanopoulou and Jason B. Siegel are with the Department of Mechanical Engineering, University of Michigan, Ann Arbor (corresponding author: Ting Cai, e-mail: tingcai@umich.edu)

978-1-5386-8266-1/$31.00 ©2020 AACC

demonstrate the effectiveness of the proposed algorithm in detecting a hard ISC event.

II. Challenges of ISC Detection

Conventional methods of ISC detection, including voltage based methods and temperature based methods, face challenges as the number of cells in the battery packs increases. Detailed analysis will be given for the voltage based method and temperature based method.

A. Voltage Detection Analysis

For parallel connected batteries, an ISC event can be difficult to identify. The following analysis for a battery pack with 50 cells in parallel represents an electric vehicle battery pack. Each of the cells in the pack is an Li-ion pouch cell with 4.5 Ah capacity. In this study, we uses an OCV-R-RC equivalent circuit model to represent the pouch cell, as shown by Fig. 1. The detailed cell model parameter is shown in Table I, which is measured from the pouch cell manufactured by University of Michigan Battery Lab.

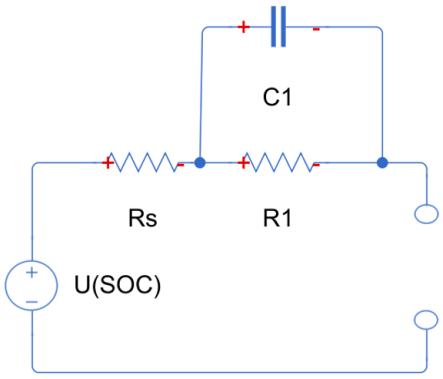

Fig. 1: Equivalent circuit model representing the cell

TABLE I: Cell Specification

Capacity	R_s	R_1	C_1
$4.5Ah$	$5.3m\Omega$	$10.4m\Omega$	$4.81 \times 10^3 F$

For single cell, after an ISC event, the terminal voltage experiences a significant drop. Since the large ISC current, the changes in State of Charge (SOC) has to be taken into consideration. The battery open circuit voltage $V(SOC)$ is a function of SOC. The following equations describe the model for the terminal voltage (V_T)

$$V_T = V(SOC) - IR_s - V_1 \tag{1}$$

$$\frac{dV_1}{dt} = \frac{-V_1}{R_1 C_1} + \frac{I}{C_1} \tag{2}$$

$$\frac{dSOC}{dt} = -\frac{I}{C_{cell}} \tag{3}$$

where C_{cell} represents the cell capacity.

For cell triggering a hard internal short with internal short resistance of $30m\Omega$, the simulation result is shown in Fig. 2. The blue solid line represents single cell voltage, and the red dashed line represents the battery pack voltage.

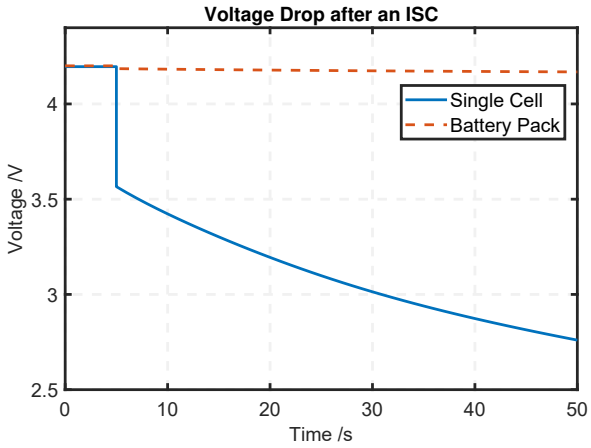

Fig. 2: Terminal voltage drop after an ISC event for a single cell and a battery pack (50 cells in parallel)

For the single cell case, the voltage drop is significant after a hard internal short. This voltage drop can be easily detected. For the battery pack with 50 cells in parallel, after the ISC, the measured terminal voltage drop will be much smaller. The instantaneous voltage drop is around $15mV$, and after 50 seconds, the total voltage drop is $32mV$. With voltage noise standard deviation being set as $\sigma_V = 5mV$ [12], the voltage drop is then at similar magnitude with voltage sensor noise with even more cells. With the increase of parallel connected cells number in a battery pack, it is even more challenging to detect an ISC event by voltage alone.

B. Temperature Detection Analysis

During normal operating conditions, there exists temperature gradient in the battery core and surface [18]. In an ISC event, the temperature gradient will be larger due to the higher local rate of heat release which results in a fast temperature increase of cell core region [14]. The ISC happens at battery core regions first, and it takes time for the battery surface to heat up. The following analysis for battery surface temperature measurement shows that the temperature detection method has its limitation in estimating ISC core temperature.

The battery cell can be divided into three regions, core, middle layer and surface layer [14]. The thermal model can be written as

$$C_p m_{core} \frac{dT_{core}}{dt} = (\dot{Q}_{exo,core} + \dot{Q}_{ohmic,core}) + \frac{T_{mid} - T_{core}}{r_{c2m}} \tag{4}$$

$$C_p m_{mid} \frac{dT_{mid}}{dt} = (\dot{Q}_{exo,mid} + \dot{Q}_{ohmic,mid}) - \frac{T_{mid} - T_{core}}{r_{c2m}} + \frac{T_{surf} - T_{mid}}{r_{m2s}} \tag{5}$$

$$C_p m_{surf} \frac{dT_{surf}}{dt} = (\dot{Q}_{exo,surf} + \dot{Q}_{ohmic,surf}) + \frac{T_{amb} - T_{surf}}{r_{s2a}} - \frac{T_{surf} - T_{mid}}{r_{m2s}} \quad (6)$$

where T_{core}, T_{mid}, T_{surf} represent core, middle layer and surface temperature. m_{core}, m_{mid}, m_{surf} represent mass of core, middle layer and surface. r_{c2m}, m_{m2s}, m_{s2a} represent thermal resistance of core to middle layer (c2m), middle layer to surface (m2s) and surface to ambient (s2a). Q_{exo} is the exothermic side reactions heat, Q_{ohmic} is the ohmic heat from ISC.

At the first few seconds of ISC process, T_{core} quickly rise to $120°C$ (driven by the ohmic heating in the short circuit), while T_{mid} and T_{surf} remain at $57.5°C$ [14]. The system is linearized at this point to asses the surface temperature detection method. At this working condition, exothermic reaction heat and ohmic heat in middle layer and surface can be neglected.

For the exothermic reactions, Solid Electrolyte Interface (SEI) decomposition becomes active above 120°C [1]. Comparing to ISC ohmic heat, exothermic reaction heat can be neglected at this temperature, but must be included as the cell temperate continues to rise because the reaction rate will increase exponentially with temperature [19].

The thermal model can be represented in state space representation form

$$\begin{bmatrix} \dot{T}_{core} \\ \dot{T}_{mid} \\ \dot{T}_{surf} \end{bmatrix} = A \begin{bmatrix} T_{core} \\ T_{mid} \\ T_{surf} \end{bmatrix} + \begin{bmatrix} \dot{Q}_{ohmic,core} \\ 0 \\ \frac{T_{amb}}{C_p m_{surf} r_{s2a}} \end{bmatrix} \quad (7)$$

$$y = C \begin{bmatrix} T_{core} \\ T_{mid} \\ T_{surf} \end{bmatrix} \quad (8)$$

where $C = [0, 0, 1]$ and the output here is the surface temperature.

In details, the A matrix is

$$A = \begin{bmatrix} A_{11} & A_{12} & 0 \\ A_{21} & A_{22} & A_{23} \\ 0 & A_{32} & A_{33} \end{bmatrix}$$

where $A_{11} = -\frac{1}{C_p m_{core} r_{c2m}}$, $A_{12} = \frac{1}{C_p m_{core} r_{c2m}}$ $A_{21} = \frac{1}{C_p m_{mid} r_{c2m}}$, $A_{22} = -\frac{r_{c2m}+r_{m2s}}{r_{c2m} r_{m2s} C_p m_{mid}}$, $A_{23} = \frac{1}{C_p m_{mid} r_{m2s}}$ $A_{32} = \frac{1}{C_p m_{surf} r_{m2s}}$, $A_{33} = -\frac{r_{m2s}+r_{s2a}}{r_{m2s} r_{s2a} C_p m_{surf}}$

For system with surface temperature as the only output, the observability matrix is

$$Q = \begin{bmatrix} C \\ CA \\ CA^2 \end{bmatrix} \quad (9)$$

Take the numerical values from the modeling result [14]. We have the observability matrix expressed as

$$Q = \begin{bmatrix} 0 & 0 & 1 \\ 0 & 0.0058 & -0.015 \\ 3.52 \times 10^{-4} & -0.0011 & 9.22 \times 10^{-4} \end{bmatrix} \quad (10)$$

The observability matrix is full rank, which means the system is observable with the surface temperature output alone. However, if we do Singular Value Decomposition (SVD) for the observability matrix

$$Q = U \Sigma V^* \quad (11)$$

The singular values σ_i will be given by the diagonal entries of

$$\Sigma = \begin{bmatrix} 1.0001 & 0 & 0 \\ 0 & 0.0059 & 0 \\ 0 & 0 & 0.0003 \end{bmatrix} \quad (12)$$

The observability matrix has a very high condition number

$$\kappa(Q) = \frac{\sigma(max)}{\sigma(min)} = 2892 \quad (13)$$

This shows that the observability matrix is close being rank deficient. This analysis demonstrates the poor observability for the internal temperature state based on surface temperature measurement alone. In real practice, with thermocouples located only at a few spots in a battery pack, the temperature response will be even slower. Better approaches are needed to identify the ISC event.

III. ISC Detection based on Force

Previous studies [14] on single cell triggering hard internal short showed the relative slow response of surface temperature, and fast response of voltage and expansion force. The expansion force comes from the cell swelling due to gas generation. The SEI decomposition becomes active at around $120°C$ [1], and follows the expression below [1]

$$(CH_2OCO_2Li)_2 \rightarrow Li_2CO_3 + C_2H_4 + CO_2 + 0.5O_2$$

The SEI decomposition directly generate gas that can contribute to severe cell swelling. The cell swelling converts to expansion signal. The expansion force, due to its fast response after a hard internal short, can be used for ISC detection.

A. Expansion Force Measurements in Battery Packs

In battery packs, similar to the one shown in Fig. 3, the expansion of one cell in the stack also results in an increase in the total expansion of the stack, which can be measured using the total stress on the module.

Fig. 3: Battery module with closely stacked cells

In battery packs, the expansion force can be used to detect a battery fault since the stress will be translated to the fixture as a serial topology, even though the cells are electrically connected in parallel. In the following discussion, a single cell ISC detection algorithm is discussed as an example, but the methodology also applies to battery packs.

B. Expansion Force Model

At normal operating conditions, the cell expansion force can be expressed as a function of temperature and State of Charge (SOC). Previous studies showed the change of cell expansion force from fully discharged to fully charged state is around 35 pounds or 30% of the base preload for NMC-Graphite cells [20]. Compared to the peak force observed prior to venting during a thermal event, which was over 400 pounds [14], the expansion due to SOC is small. We assume the temperature dependency and SOC dependency functions are separable [21]. We can then express the expansion force as

$$F = f_1(T) + f_2(SOC) \tag{14}$$

For the SOC dependency, the experiment of expansion force measurement uses the same setting as in [20]. The experiment settings for expansion force measurement are shown in Fig 4a. The expansion force measurement comes from the four load cells at four corners of the fixture. We use a eighth order of polynomial fit for the experimental data. The resulted expansion force with SOC dependency is shown in Fig 4b.

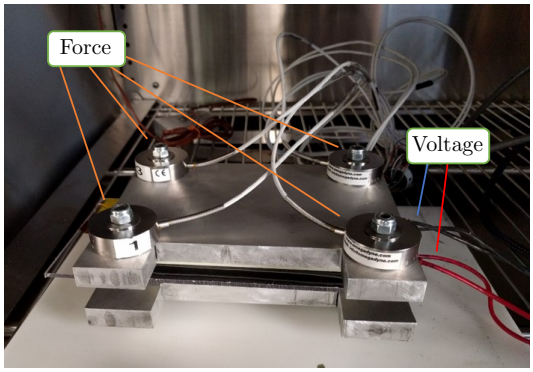

Fig. 4a: Expansion force measurement setup

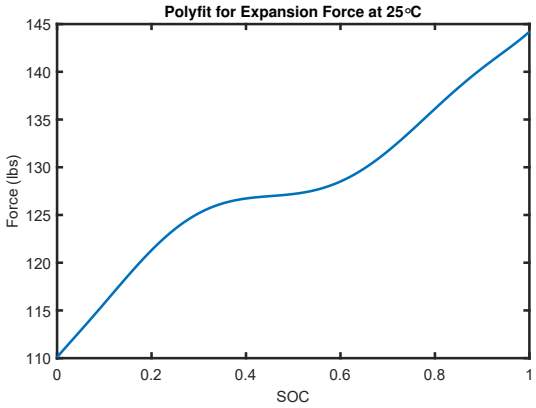

Fig. 4b: Expansion force as a function of SOC

For the temperature dependency, here we use a linear thermal expansion model for the expansion force. The temperature dependency can be expressed as

$$f_1(T) = \alpha(T - T_0) \tag{15}$$

where T_0 is the initial temperature, and α is the thermal expansion rate. For α, different fixture and battery will have different thermal expansion coefficient. Here, we calculate it based on the expansion force for the pouch cell at different temperature. The α in this study is $0.464\ lbf/°C$

During normal operating conditions, temperature distribution is rather uniform within a cell. The measured surface temperature can be used in the thermal expansion model.

Other factors that impact expansion force include pre-load force. We assume local linearization for the force model that allows the separation of temperature, SOC and pre-load [21]. With pre-load force included in the model, the expansion force during normal operating conditions can then be expressed as

$$F = f_1(T) + f_2(SOC) + F_0 \tag{16}$$

where F_0 is the pre-load force.

C. Fault Detection Algorithm

Based on the expansion force model at normal operating conditions, we can build an observer for the expansion force

$$\hat{F} = f_1(T) + f_2(\hat{SOC}) + F_0 + \hat{\Theta} \tag{17}$$

$$\dot{\hat{\Theta}} = L(\bar{F} - \hat{F}) \tag{18}$$

where $\bar{F}$ is the measured force, and $\hat{\Theta}$ is the estimated fault force signal. The estimated fault force signal from internal short is then calculated from force measurement and estimated expansion force.

Here, we assume the $\hat{SOC}$ can be estimated by current and voltage measurement. Common methods for SOC estimation include Coulomb Counting method and Open Circuit Voltage inversion method. Coulomb Counting method is more popular in industry, as the battery terminal voltage changes in dynamic operations [20]. SOC estimation error can come from sensor noise and drift, model mismatch due to cell aging [22]. A 5% error in the estimated SOC would result in a prediction error of 2 lbf for $\hat{\Theta}$, based on the maximum slope in figure 4b. Even though this error for $\hat{\Theta}$ is acceptable, closed loop SOC estimation is desired to achieve better performance in real practice. To simplify the analysis here, we will use Coulomb Counting only method for SOC estimation in this study.

At normal operating conditions, the force measurement should be equal to the estimated expansion force, and Θ should ideally be zero. The F_{fault} term represents the force that comes from battery swelling due to an internal short. To put the two cases in summary:

During Normal Conditions

$$\bar{F} = f_1(T) + f_2(SOC) + F_0$$

$$\hat{F} = f_1(T) + f_2(\hat{SOC}) + F_0 + \hat{\Theta}$$

$$\hat{\Theta} \to 0$$

At Fault Conditions

$$\bar{F} = f_1(T) + f_2(SOC) + F_0 + F_{fault}$$
$$\hat{F} = f_1(T) + f_2(\hat{SOC}) + F_0 + \hat{\Theta}$$
$$\hat{\Theta} \rightarrow F_{fault}$$

The detection quantity $\hat{\Theta}$ converges to zero during normal operating conditions. At fault conditions, the detection quantity $\hat{\Theta}$ converges to the fault force signal. Thus, the detection algorithm can be written as

$$\left|\hat{\Theta}\right| \begin{cases} \leq \epsilon_F, & \text{Normal} \\ > \epsilon_F, & \text{ISC Alert.} \end{cases} \tag{19}$$

where ϵ_F is the predefined threshold. A smaller threshold may lead to improved detectability of the fault, however, this will bring higher false alarm rates.

D. Higher Confidence Level Detection

For higher confidence level detection, we can use multiple detection algorithms from different input measurement. If each of the detection algorithm indicates an alert, then an ISC alert will be made. If only some of the sensors indicate ISC warning, then this might be sensor error.

The voltage detection method works well in the single-cell case or battery packs with only a few parallel connected cells. As the number of parallel-connected cells in the pack increases, fault detection based on the voltage signal will become more difficult. Therefore, including the expansion force signal improve fault detection results in a higher confidence level. As in [6], we define the fault voltage as

$$V_{fault} = V_{normal} - \bar{V} \tag{20}$$

where $\bar{V}$ is the measured voltage, and V_{normal} is the cell voltage at normal operating conditions. The V_{normal} term can be calculated from R-RC equivalent circuit model as described in Fig. 1.

If the fault voltage value exceeds the pre-defined value ϵ_V, then the voltage detection system will trigger an alarm. After receiving alarms from both force and voltage, an ISC event is believed to happen. In a summary:

TABLE II: Detection Logic

Voltage	Force	Decision
$V_{fault} > \epsilon_V$	$\hat{\Theta} > \epsilon_F$	ISC Alert
$V_{fault} > \epsilon_V$	$\hat{\Theta} < \epsilon_F$	Sensor Error
$V_{fault} < \epsilon_V$	$\hat{\Theta} > \epsilon_F$	Sensor Error
$V_{fault} < \epsilon_V$	$\hat{\Theta} < \epsilon_F$	Normal

IV. Simulation Result

For this study, we consider a 4.5 Ah NMC pouch cell. The parameters of the cell are adopted from [14]. To emulate real measurements, here, we add zero mean white Gaussian noise ($N(0, \sigma^2)$) to the measurement. In details, for voltage measurement, the noise has covariance $\sigma_V = 5\ mV$. For current measurement, $\sigma_I = 5\ mA$. For temperature measurement, $\sigma_T = 0.5\ ^\circ C$. For force measurement, $\sigma_F = 2\ lbf$.

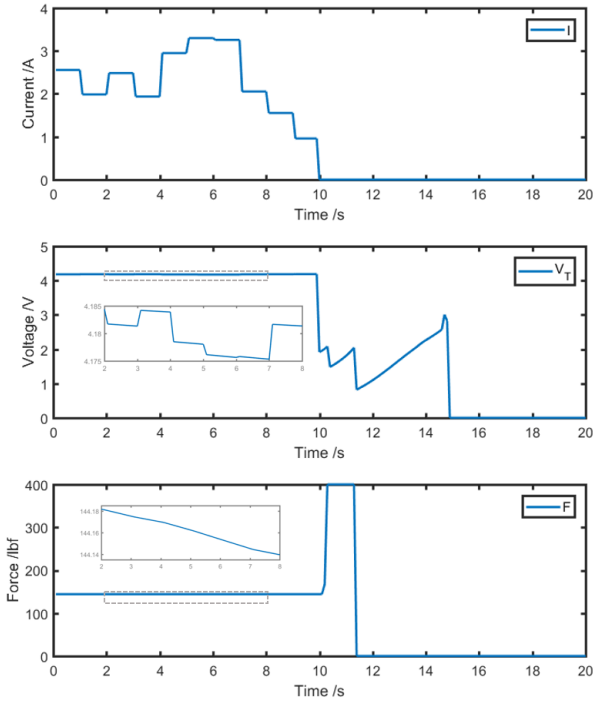

Fig. 5a: Current, terminal voltage and expansion force profile under a fault condition, with a hard short circuit triggered at $t = 10s$

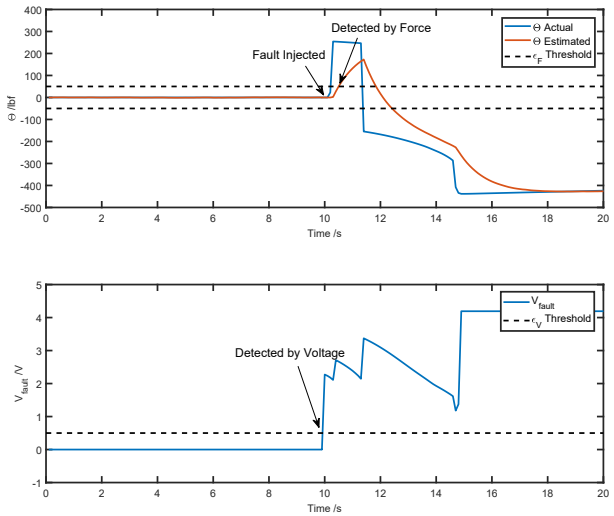

Fig. 5b: At fault conditions, voltage detection V_{fault} identifies a fault at $t = 10s$, and force detection $\hat{\Theta}$ confirms the fault at $t = 10.5s$

The simulation can be divided into two regions: normal operating conditions and after the fault triggered, fault conditions. In the normal operating conditions, the Urban Dynamomenter Driving Schedule (UDDS) is used for the current profile. In the fault condition, the model from [14] is used to simulate a hard ISC case. For the detection threshold,

voltage detection threshold is set to $\epsilon_V = 0.5V$, and force detection threshold is set to $\epsilon_F = 100\ lbf$.

The battery SOC is initialized at $SOC = 1$ in the simulation. For the first 10 seconds under normal operating conditions, the UDDS current profile and the corresponding terminal voltage (V_T) and expansion force responses have been shown in Fig. 5a. During normal operating conditions, both detection quantities stay far below the detection threshold. Even with measurement noise added, no false alarms is triggered during the simulation.

At $t = 10s$, an ISC is triggered in the simulation which finally leads to a thermal runaway event. After the ISC event, we assume there is no external current flowing through the cell. The model from [14] is adopted to simulate a hard short which leads to a thermal runaway event. The simulated hard ISC event is shown in Fig. 5a for the current, voltage and force profile.

The estimated voltage fault term V_{fault}, estimated force fault term $\hat{\Theta}$ and the actual Θ after a short circuit triggered are shown in Fig. 5b. At the time of 10 seconds, the voltage fault term first detects an ISC event. At the time of 10.5 seconds, the force detection algorithm identifies the fault, and confirms the ISC event. Even though the confirmation of an ISC event requires threshold crossing from both voltage and force detection signals, it still achieves fast detection for a hard internal short event.

To be noticed, in Fig. 5b, at the time of 12.5 seconds, the $\hat{\Theta}$ drops below the lower threshold $-50\ lbf$, and triggers the alarm for the second time. This is due to the rupture of the cell, which leads to sudden drop of measured expansion force. The increase of surface temperature also follows the rupture and thermal runaway. These two factors cause the $\hat{\Theta}$ to drop below the lower threshold $-50\ lbf$. This feature makes the force detection to continually identify this fault even after a long time of triggering the fault.

V. Conclusion

In this paper, we propose a battery ISC detection method based on the measurement of the expansion force and voltage. Combining voltage and force signals for fault estimation can achieve a higher confidence level for detection of the fault and avoid unnecessary false alarms. The simulation results demonstrate the fast response of the detection algorithm after an ISC event. The simulation also verified that the method is robust to sensor noise. Future work is needed with experimental validation for the detection method.

Acknowledgment

This work is supported by the National Science Foundation under Grant No. 1762247. The author wish to acknowledge Miriam Figueroa for assistance with UDDS current profile.

References

[1] X. Feng, M. Ouyang, X. Liu, L. Lu, Y. Xia, and X. He, "Thermal runaway mechanism of lithium ion battery for electric vehicles: A review," *Energy Storage Materials*, vol. 10, pp. 246–267, 2018.

[2] R. Spotnitz and J. Franklin, "Abuse behavior of high-power, lithium-ion cells," *J. Power Sources*, vol. 113, no. 1, pp. 81–100, 2003.

[3] S. Abada, G. Marlair, A. Lecocq, M. Petit, V. Sauvant-Moynot, and F. Huet, "Safety focused modeling of lithium-ion batteries: A review," *J. Power Sources*, vol. 306, pp. 178–192, 2016.

[4] X. Feng, M. Fang, X. He, M. Ouyang, L. Lu, H. Wang, and M. Zhang, "Thermal runaway features of large format prismatic lithium ion battery using extended volume accelerating rate calorimetry," *J. Power Sources*, vol. 255, pp. 294–301, 2014.

[5] M. Zhang, L. Liu, A. Stefanopoulou, J. Siegel, L. Lu, X. He, and M. Ouyang, "Fusing phenomenon of lithium-ion battery internal short circuit," *J. Electrochem. Soc.*, vol. 164, no. 12, pp. A2738–A2745, 2017.

[6] B. Xia and C. Mi, "A fault-tolerant voltage measurement method for series connected battery packs," *Journal of Power Sources*, vol. 308, pp. 83–96, 2016.

[7] B. Xia, Y. Shang, T. Nguyen, and C. Mi, "A correlation based fault detection method for short circuits in battery packs," *Journal of power Sources*, vol. 337, pp. 1–10, 2017.

[8] M. Zhang, J. Du, L. Liu, A. Stefanopoulou, J. Siegel, L. Lu, X. He, X. Xie, and M. Ouyang, "Internal short circuit trigger method for lithium-ion battery based on shape memory alloy," *J. Electrochem. Soc.*, vol. 164, no. 13, pp. A3038–A3044, 2017.

[9] M. Zhang, J. Du, L. Liu, J. Siegel, L. Lu, X. He, and M. Ouyang, "Internal short circuit detection method for battery pack based on circuit topology," *Science China Technological Sciences*, vol. 61, no. 10, pp. 1502–1511, 2018.

[10] X. Feng, C. Weng, M. Ouyang, and J. Sun, "Online internal short circuit detection for a large format lithium ion battery," *Appl. Energy*, vol. 161, pp. 168–180, 2016.

[11] S. Dey, H. E. Perez, and S. J. Moura, "Model-based battery thermal fault diagnostics: Algorithms, analysis, and experiments," *IEEE Transactions on Control Systems Technology*, vol. 27, no. 2, pp. 576–587, 2017.

[12] S. Dey, Y. Shi, K. Smith, and M. Khanra, "Safer batteries via active fault tolerant control," in *2019 American Control Conference (ACC)*. IEEE, 2019, pp. 1561–1566.

[13] T. Cai, A. Stefanopoulou, and J. Siegel, "Modeling li-ion battery thermal runaway using a three section thermal model," in *Dynamic Systems and Control Conference*. ASME, 2018.

[14] T. Cai, A. G. Stefanopoulou, and J. B. Siegel, "Modeling li-ion battery temperature and expansion force during the early stages of thermal runaway triggered by internal shorts," *Journal of The Electrochemical Society*, vol. 166, no. 12, pp. A2431–A2443, 2019.

[15] Z. Liao, S. Zhang, K. Li, G. Zhang, and T. G. Habetler, "A survey of methods for monitoring and detecting thermal runaway of lithium-ion batteries," *Journal of Power Sources*, vol. 436, p. 226879, 2019.

[16] M. Lammer, A. Königseder, and V. Hacker, "Holistic methodology for characterisation of the thermally induced failure of commercially available 18650 lithium ion cells," *RSC Advances*, vol. 7, no. 39, pp. 24 425–24 429, 2017.

[17] T. Cai, A. G. Stefanopoulou, and J. B. Siegel, "Early detection for li-ion batteries thermal runaway based on gas sensing," *ECS Transactions*, vol. 89, no. 1, pp. 85–97, 2019.

[18] X. Lin, H. E. Perez, J. B. Siegel, A. G. Stefanopoulou, Y. Li, R. D. Anderson, Y. Ding, and M. P. Castanier, "Online parameterization of lumped thermal dynamics in cylindrical lithium ion batteries for core temperature estimation and health monitoring," *IEEE Transactions on Control Systems Technology*, vol. 21, no. 5, pp. 1745–1755, 2013.

[19] P. T. Coman, E. C. Darcy, C. T. Veje, and R. E. White, "Modelling li-ion cell thermal runaway triggered by an internal short circuit device using an efficiency factor and arrhenius formulations," *J. Electrochem. Soc.*, vol. 164, no. 4, pp. A587–A593, 2017.

[20] T. Polóni, M. A. Figueroa-Santos, J. B. Siegel, and A. G. Stefanopoulou, "Integration of non-monotonic cell swelling characteristic for state-of-charge estimation," in *2018 Annual American Control Conference (ACC)*. IEEE, 2018, pp. 2306–2311.

[21] S. Mohan, Y. Kim, J. B. Siegel, N. A. Samad, and A. G. Stefanopoulou, "A phenomenological model of bulk force in a li-ion battery pack and its application to state of charge estimation," *Journal of the Electrochemical Society*, vol. 161, no. 14, pp. A2222–A2231, 2014.

[22] P. Mohtat, S. Lee, J. B. Siegel, and A. G. Stefanopoulou, "Towards better estimability of electrode-specific state of health: Decoding the cell expansion," *Journal of Power Sources*, vol. 427, pp. 101–111, 2019.